Journal of Solid State Chemistry **150,** 178–182 (2000)
doi:10.1006/jssc.1999.8574, available online at http://www.idealibrary.com on IDEAL®

Optical Spectroscopy Properties and Charge Compensation of $BaLiF_3$ Doped with Ce^{3+}

Yiwei Tan and Chunshan Shi[1]

Laboratory of Rare Earth Chemistry and Physics, Changchun Institute of Applied Chemistry, Chinese Academy of Science, Changchun, 130022, People's Republic of China

Received June 28, 1999; in revised form October 20, 1999; accepted November 5, 1999

The excitation and emission spectra of the $BaLiF_3:Ce^{3+}$ phosphors synthesized through solid state reaction have been measured. By investigating the properties of the excitation spectra we point out that the variation in the excitation spectra with the amount of CeF_3 dopant results from the different patterns of charge compensation in the matrices. The vacancies of Li^+ ions are the favorable charge compensation pattern at low concentration of CeF_3 doped, but interstitial F^- ions are the major charge compensation pattern when the concentration of CeF_3 doped goes beyond a certain value.

Key Words: **$BaLiF_3$; Ce^{3+}; photoluminescence; charge compensation.**

INTRODUCTION

The phosphors activated by Ce^{3+} are of great value in optical materials. On one hand, the broad UV emission from $5d$–$4f$ transition makes it possible to develop a tunable short-wave solid state laser (1–2), amplifier (3), efficient scintillator (4–5), and sensitizer (6). On the other hand, the Ce^{3+} ion possessing one single electron hosted in wide band-gap crystals makes it possible for a complete study of all its spectroscopy properties. Previously, the fluoride materials used to study the Ce^{3+} luminescent properties mainly focused on the alkaline earth and perovskite complex fluoride. Although $BaLiF_3:Ce^{3+}$ crystals recently have been studied as thermal neutron scintillation detector (7–8), to our knowledge, there have been up to now few reports about the studies on photoluminescence of $BaLiF_3:Ce^{3+}$. In this article, we investigate and discuss the charge compensation of Ce^{3+} substitutional ions according to the fluorescence properties of $BaLiF_3:Ce^{3+}$.

A schematic diagram of levels of the Ce^{3+} ion in different symmetries is drawn in Fig. 1. In this figure, the free-ion calculated levels according to Dieke (9) are shown on the left-hand side. The spin–orbit interaction splits the $4f$ ground state into two levels $^2F_{7/2}$ and $^2F_{5/2}$, separated by 2253 cm^{-1}; the $5d$ level approximately 51,000 cm^{-1} above the ground state is split into $^2D_{5/2}$ and $^2D_{3/2}$ distant about 1000 cm^{-1}; the $6s$ level is at about 86000 cm^{-1}. For the Ce^{3+} ion, as we shall see below, a cubo-octahedral site is the most probable substitutional site. The $5d$ level is split into the two e_g and t_{2g} bands in the order as indicated by the crystal field. If a weak spin–orbit interaction is further applied, the t_{2g} level should further split into the Γ_7 and Γ_8 components. In the case of a large crystal field of lower symmetry, for example, that produced by the presence of charge compensating interstitials or cation vacancies, the degeneracy of the $5d$ level is completely removed as shown by the five Kramers doublets on the right-hand side of Fig. 1. The total splitting of the $5d$ manifold varies in the different fluoride host from 7000 to 14000 cm^{-1}, and therefore the effects of the crystal field are much larger than those of the spin–orbit interaction.

The inverted perovskite $BaLiF_3$ crystallizes in a cubic phase whose space group is O_h^1 or P_{m3m} and the lattice parameter is 3.995 Å (10). Ba^{2+} and Li^+ occupy inverted position as compared with other fluoroperovskites such as $KZnF_3$: the divalent Ba^{2+} ions are located at the corners of a cube and the Li^+ ions are at the center of the fluorine octahedron.

EXPERIMENTAL

Synthesis

The starting materials are metal fluorides, i.e., (BaF_2 (analysis purity), LiF (analysis purity), CeF_3 (99.9%). Each component is weighed precisely according to the amount of CeF_3 doped in the $BaLiF_3$. The raw materials are first thoroughly ground in an agate mortar. Then the mixture is put into a corundum crucible and fired in the constant temperature zone of a tube-type furnace. The temperature is raised slowly to 350°C and kept at that temperature for 2 h to remove any water that might be contained in the raw materials. Then the temperature is raised to 750°C slowly

[1] To whom correspondence should be addressed.

0022-4596/00 $35.00

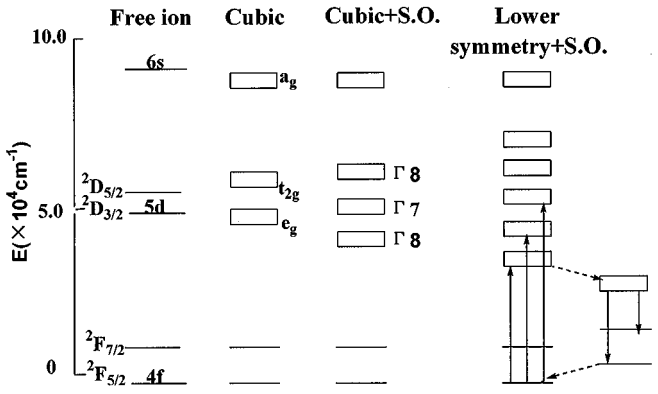

FIG. 1. Schematic energy levels of the Ce^{3+} ion. Levels on the right represent the ion in a symmetry lower than cubic (perturbed site) with the relevant optical transition indicated by solid arrows (radiative) and dashed arrows (nonradiative).

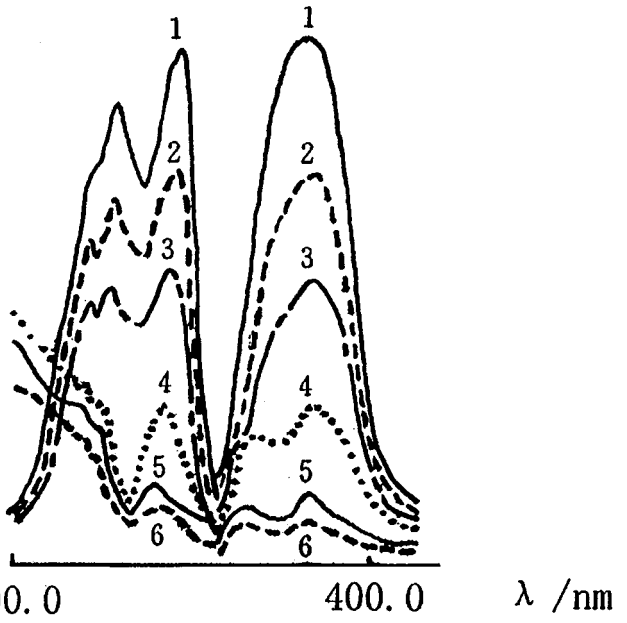

FIG. 2. Excitation ($\lambda_{em} = 361$ nm) and emission ($\lambda_{ex} = 291$–301 nm) spectra of $BaLiF_3:xCe^{3+}$ phosphors (1) $x = 0.05\%$; (2) $x = 0.2\%$; (3) $x = 0.4\%$; (4) $x = 0.6\%$; (5) $x = 0.8\%$; (6) $x = 1.0\%$.

and kept at that temperature for 5 h. The samples are then cooled to room temperature. The whole process is in a N_2 atmosphere. White sintered powders are obtained at last. Part of the product is annealed to 600°C in air and kept at that temperature for 1 h. The same synthesizing procedure mentioned above is carried out with the raw materials which have not been dried in advance.

Physical Measurements

All above-prepared $BaLiF_3:Ce^{3+}$ crystallites were checked by X-ray diffraction and were in good agreement with JCPDS No. 18-715. The excitation and emission spectra were measured with a Japan Shimadazu RF-5000 fluorescence spectrophotometer at room temperature. The oxygen content in $BaLiF_3:Ce^{3+}$ was determined by a VG ESCA LADMT X-ray photoelectron spectrometer. All measurements were carried out at room temperature.

RESULTS AND DISCUSSION

Spectra of $BaLiF_3:Ce^{3+}$

Figure 2 shows the excitation and emission spectra of the samples of $BaLiF_3:xCe^{3+}$ crystallite powders ($x = 0.05, 0.2,$ 0.4, 0.6, 0.8, and 1.0%) whose raw materials have been dried. The excitation wavelength is selected in the long wavelength region (291–301 nm). Table 1 summarizes the locations of each peak. From Fig. 2. it can be clearly observed that double broad emission bands appear peaking at 328 and 361 nm, respectively, when the concentration of CeF_3 doped is relatively low ($\leq 0.4\%$), which are characteristics of Ce^{3+} $4f^05d^1 \rightarrow {}^2F_{5/2}$ and ${}^2F_{7/2}$ electric dipole-allowed transition. Within the range of above-mentioned concentration the band intensity of both wavelength regions increases accompanied by the amount of the CeF_3 dopant. The separation between the two regions is about 2700 cm^{-1}. It is a slightly higher value compared with the free–Ce^{3+} ion value corresponding to distance between ${}^2F_{5/2}$ and ${}^2F_{7/2}$. As the concentration of Ce^{3+} ion increases, we find that the 328-nm emission intensity gradually decreases, causing the shoulder peak to vanish. Conversely, the 361-nm emission intensity gradually increases. Concentration quenching is not found

TABLE 1
The Excitation and Emission Wavelengths (nm) of $BaLiF_3:Ce^{3+}$ at Room Temperature

The amount of dopant CeF_3 (mol%)	0.05	0.2	0.4	0.6	0.8	1.0
Excitation wavelength	< 200, 234, 254, 291	< 200, 235, 254, 291	< 200, 237, 250, 291	243, 257, 297	243, 257, 297	245, 257, 301
Emission wavelength	328, 361	328, 361	328, 361	328,[a] 361	361	361

[a] Shoulder peak.

in the scope of this experimental research. The shape of the emission band changes a little when shorter wavelength UV is used to excite the samples. The width of the emission band narrows but the location remains unchanged. In Fig. 2 we can easily observe that excitation spectra consist of two regions with a monitoring wavelength at 361 nm: the relatively weak and broad band A from 230 nm extending to below 200 nm is present at low CeF_3 concentrations (not more than 0.4 mol%); three bands appear between 235 and 320 nm within the whole dopant concentration range, called region B. This suggests that the 5*d* level is split by the crystal field into five levels. Within the limits of resolving power of the spectrometer or weak intensity of some absorption bands we cannot see all of the excitation peaks.

Investigation of Charge Compensation in $BaLiF_3 : Ce^{3+}$ Phosphors

The spectroscopic characters of Ce^{3+} ion greatly depend on the host crystal-field strength and the symmetry of the crystal site. In $BaLiF_3$ the charge number and ionic radius of Ce^{3+} (1.03 Å) are all closer to Ba^{2+} charge number and radius (1.35 Å) than those of Li^+ (0.60 Å). It is more likely for the substitutional Ce^{3+} ion to be on the Ba^{2+} site (8). Due to the nonequivalent substitution, an excess of positive charge in the lattice must be compensated for, which can take place in a series of ways, including the following:

1. introduction of a Li^+ vacancy;
2. formation of a F^- interstitial;
3. O^{2-} substitution at a F^- site;
4. Li^+ substitution at a Ba^{2+} site (near a Ce^{3+} site);
5. formation of a Ba^{2+} vacancy (compensates for two substitutions);
6. other impurity ions used as compensators.

Whichever case of charge compensation exists, the symmetry of the Ce^{3+} site is lowered from cubic to C_{3v}, C_{4v} or lower site symmetries. First, we believe the possibility of O^{2-} as charge compensator is minor, given the high purity of dopant CeF_3. Moreover, the solid state reaction is carried out in a high-purity N_2 atmosphere in the hermetically sealed chamber. Second, the Li^+ substitution at a Ba^{2+} site (Li'_{Ba}) close to a Ce^{3+} site will result in lattice distortion due to the great disparity between Li^+ and Ba^{2+} radii. So the energy of this defect formation is great (11.47 eV) (11). We infer two charge compensation patterns assigned to low and high Ce^{3+} concentration in host, respectively, from the excitation spectra of $BaLiF_3$ doped with different amounts of CeF_3. That is to say, there are two models of luminescent Ce^{3+} centers, which are shown in Fig. 3. The excitation spectra extending to below 200 nm with a photon energy maximum above 50000 nm^{-1} can be interpreted as a transition from 4*f* to the uppermost level of 5*d*. Only when Li^+ vacancies (V'_{Li}, i.e., V_k center) are used as charge compensators can the small crystal field repulsive force form and large space be provided for the single 4*f* level electron of Ce^{3+} transition to the place which is far from the nucleus. Another case of Ba^{2+} vacancies (V''_{Ba}) compensation for two substitutions should also be taken into account. However, V''_{Ba} as a charge compensator is unfavorable because the energy of V''_{Ba} formation (18.86 eV) is higher than that of two

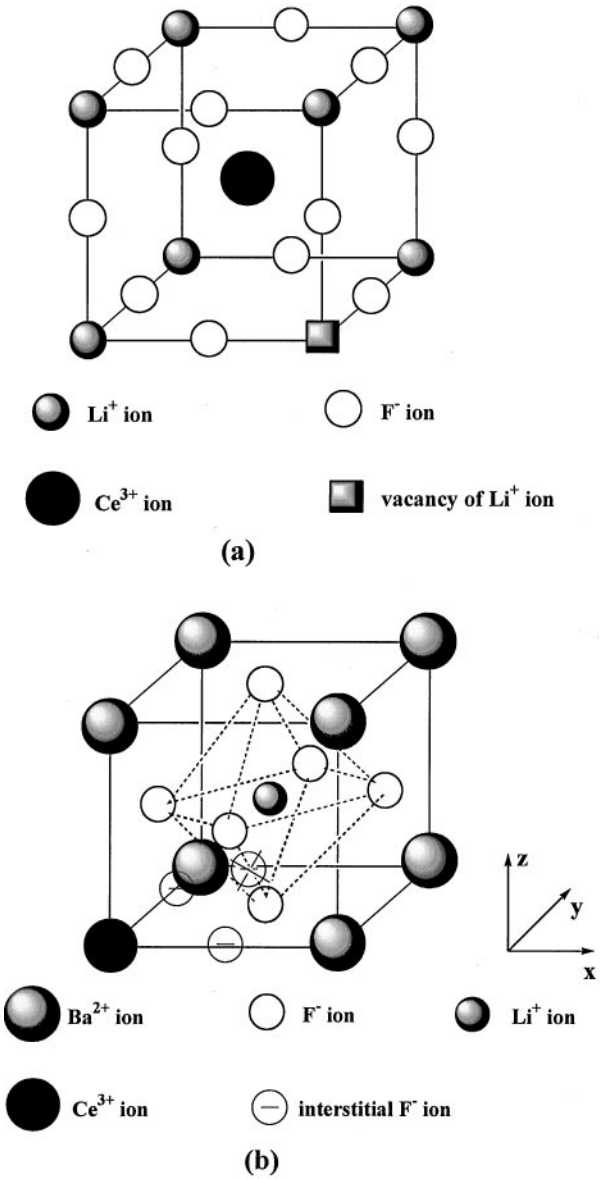

FIG. 3. Two models of luminescent Ce^{3+} centers in $BaLiF_3$: (a) the Li^+ vacancy on the C_{3v} axis of unit cell, (b) interstitial F^- ion in the unit cell. We define the site of the substitutional Ce^{3+} ion as the origin. The interstitial F^- should be around the Ce^{3+} ion whose radius is small. Three different interstitial F^- sites have been considered. The possible sites are (i) the center of the edge of the Ba^{2+} cube (1/2, 0, 0), (ii) the midpoint of the diagonal of the Ba^{2+} cube between a Ba^{2+} and a Li^+ ion (1/4, 1/4, 1/4). But the F^- interstitial (iii) at the center of the edge of the F^- octahedron (1/2, 1/4, 1/4) does not converge since this site is very close to two other F^- positions, leading to strong repulsion.

V'_{Li} (2×8.51 eV) formation (11). Furthermore, it is also unfavorable from the point of view of entropy, because it is comprehensible that spatial arrangement with one Ba^{2+} vacancy compensating for two residue charges of Ce^{3+} ions is more orderly than that with two Li^+ vacancies as compensators. Li^+ vacancies probably lie on the C_{3v} axis, which can be verified by two emission peaks around 590 nm of $BaLiF_3:Eu^{3+}$ (12). From the drastic variation in excitation, we can infer that as the Ce^{3+} ion concentration becomes so great that it is impossible to fulfil charge compensation completely by Li^+ vacancies; another charge compensation pattern in which interstitial F^- ions are predominant will appear. The formation of interstitial F^- ions can cause a stronger crystal-field repulsive force effect on the 5*d* level of Ce^{3+}, and even the 5*d* orbit of Ce^{3+}, to overlap with the 2*p* orbit of F^-. As a result, the intensity of the A excitation bands (below 230 nm) becomes weaker and the B excitation band exhibits a red-shift with an increase in Ce^{3+} concentration. It can be concluded that the probability of a 4*f* transition to the uppermost level of 5*d* reduces dramatically and the energy level of each split component of 5*d* is lowered. In Table 2 we attempt to assign the energy to each 5*d* component of Ce^{3+} in the $BaLiF_3$ host. But this assignment is only tentative due to the absence of more detailed information (such as through an extended X-ray absorption fine structure experiment). Meanwhile, the possibility of the Ce^{3+} ion in the perfect cubo-octahedral site with charge compensators (V'_{Li}) far from the Ce^{3+} ion is present. It is apparent that this structure quickly saturates because the vacancies introduced begin to perturb one or the other perfect cubo-octahedral site. This case is notable for Ce^{3+} at low concentration. The Ce^{3+} at a high-symmetry site has higher transition energies than at the vacancy-perturbed site. We can see this tendency from excitation spectra. The splitting width of the 5*d* manifold is about 7600 cm^{-1}.

As the Ce^{3+} concentration increases by a certain extent, a single emission band is observed. Blasse and Bril (13) originally interpreted this phenomenon as energy transfer by radiation self-absorption. However, the overlapping between the excitation and emission bands does not occur in $BaLiF_3:Ce^{3+}$. We assume that the relatively weak 328 nm band may be hidden under the continuously intensifying and broadening 361-nm band.

TABLE 2
5*d* Levels for the Ce^{3+} Ion in the Crystal Field of $BaLiF_3:xCe^{3+}$

The amount of dopant CeF_3 (mol%)	Experimental data (10^3 cm^{-1}) assignment to components of 5*d* orbit			
	x^2-y^2	z^2	xy	yz and xz
$\leq 0.4\%$	34.4	39.4	42.5	≈ 50.0
$> 0.4\%$	33.7	38.9	41.1	—

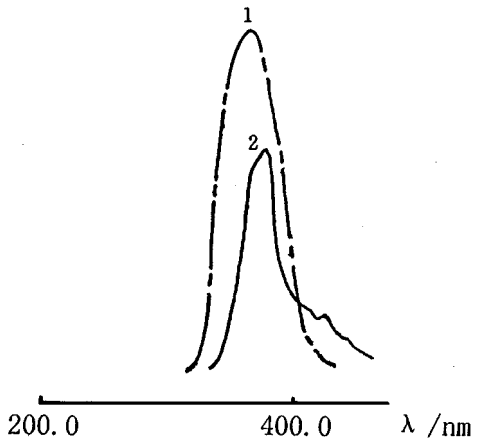

FIG. 4. The emission spectral of $BaLiF_3:Ce^{3+}$ prepared under two different conditions: (1) the starting material of $BaLiF_3:Ce^{3+}$ (CeF_3 1.0% mol) having not been dried (solid line) and (2) $BaLiF_3:Ce^{3+}$ (CeF_3 1.0 mol%) having been annealed in air (dot-dash line).

Figure 4 shows emission spectra of $BaLiF_3:Ce^{3+}$ prepared under two different conditions. One emission band with its maximum at 370 nm comes from $BaLiF_3:Ce^{3+}$ whose starting materials have not been dried in advance; the other with its maximum at 379 nm is produced by $BaLiF_3:Ce^{3+}$ which has been annealed at 600°C for 1 h in

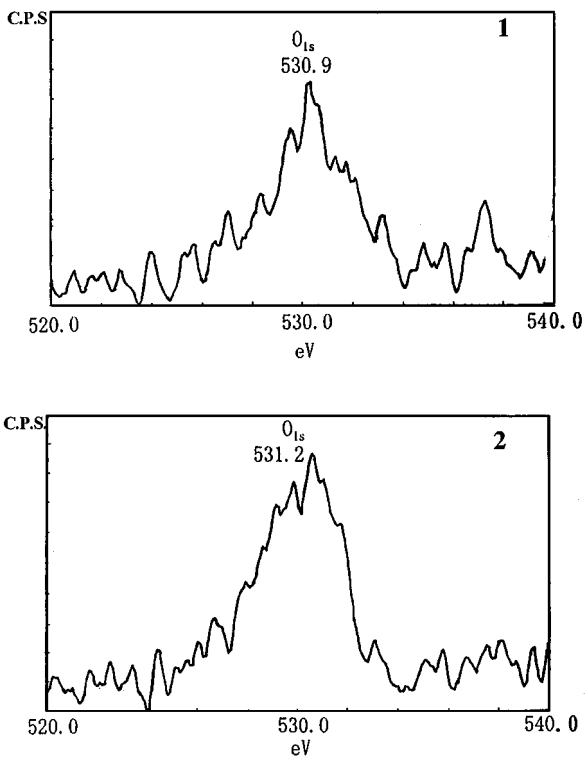

FIG. 5. ESCA of $BaLiF_3:Ce^{3+}$ (CeF_3 1.0 mol%) synthesized under different conditions: (a) $BaLiF_3:Ce^{3+}$ whose starting materials have been dried and (2) $BaLiF_3:Ce^{3+}$ which has been annealed in air.

the air, and its intensity is obviously decreased. This shows that a part of the Ce^{3+} ions have been oxidized to Ce^{4+} ions, since O^{2-} ions acting as charge compensators are imbedded in the lattice (coming from adsorbed water or air for above each case). O^{2-} ions have one more negative charge than F^- ions. The repulsive force of the crystal field increases greatly so that the $5d$ level is lowered. The $5d \rightarrow 4f$ emission of the Ce–O center shifts to a longer wavelength compared to the Ce–F center.

The oxygen content analyzed by photoelectron spectroscopy is shown in Fig. 5. Only adsorbed oxygen is obtained for $BaLiF_3:Ce^{3+}$ whose raw materials have been dried. However, not only adsorbed oxygen but also structural oxygen can be shown for $BaLiF_3:Ce^{3+}$ which has been annealed in the air.

CONCLUSION

We synthesized a series of $BaLiF_3:Ce^{3+}$ powder phosphors through solid state reaction under different reaction conditions. By the measurement of excitation and emission spectra, we hold the viewpoint that the varied Ce^{3+} concentration governs the different charge compensation procedure in the $BaLiF_3:xCe^{3+}$ system. It is not the external oxygen but the intrinsic constitution that plays the chief role in charge compensation.

ACKNOWLEDGMENT

This work is supported by the national key project for fundamental research.

REFERENCES

1. D. J. Ehrilich, P. F. Moulton, and R. M. Osgood, *Opt. Lett.* **4,** 184 (1979).
2. F. Okada, S. Togawa, K. Ohta *et al.*, *J. Appl. Phys.* **75,** 49 (1994).
3. N. Sarakura, *Opt. Lett.* **20**(3), 294 (1995).
4. C. Pedrini, B. Moine, J. C. Gacon *et al.*, *J. Phys. Condens. Matter* **4–5,** 461 (1992).
5. W. W. Moses and S. E. Derenzo, *IEEE Trans. Nucl. Sci.* **36,** 173 (1989).
6. M. J. Weber, *J. Appl. Phys.* **44**(3), 3025 (1973).
7. M. J. Knitel, P. Dorenbos, J. T. M. de Hass, and C. W. E. van Eijk, *Nucl. Instrum. Methods A* **374,** 197 (1996).
8. C. W. Combes, P. Dorenbos, C. W. E. van Eijk *et al.*, *J. Lumin.* **72–74,** 753 (1997).
9. G. H. Dieke, "Spectra and Energy Levels of Rare Earth Ions in Crystals." Wiley, New York, 1968.
10. S. Haussü hl, R. Leckebush, and K. Recker, *Z. Naturf.* **27,** 1022 (1972).
11. R. A. Jackson, M. G. M. Valerio, and J. F. de Lima, *J. Phys. Condens. Matter.* **8,** 10935 (1996).
12. Q. Su, *In* "Chemistry of Rare Earths" (J. X. Han, Ed.), p. 310. Henan Science and Technology Press, Zhengzhou, 1993.
13. G. Blasse and A. Bril, *J. Chem. Phys.* **51**(8), 3254 (1969).